

An extremely dense group of massive galaxies at the centre of the protocluster at $z = 3.09$ in the SSA22 field

M. Kubo^{1,2*}, T. Yamada,² T. Ichikawa,² M. Kajisawa,³ Y. Matsuda,^{4,5}
I. Tanaka,⁶ H. Umehata^{7,8}

¹*Institute for Cosmic Ray Research, University of Tokyo, 5-1-5 Kashiwa-no-Ha, Kashiwa City, Chiba 277-8582, Japan*

²*Astronomical Institute, Tohoku University, 6-3 Aoba, Aramaki, Aoba-ku, Sendai, Miyagi 980-8578, Japan*

³*Research Centre for Space and Cosmic Evolution, Ehime University, Bunkyo-cho 2-5, Matsuyama 790-8577, Japan*

⁴*Chile Observatory, National Astronomical Observatory of Japan, Tokyo 181-8588, Japan*

⁵*SOKENDAI (Graduate University for Advanced Studies), Osawa 2-21-1, Mitaka, Tokyo 181-8588, Japan*

⁶*Subaru Telescope, National Astronomical Observatory of Japan, 650 North A'ohoku Place, Hilo, HI 96720, USA*

⁷*European Southern Observatory, Karl-Schwarzschild-Str. 2, D-85748 Garching, Germany*

⁸*Institute of Astronomy, The University of Tokyo, Mitaka, Tokyo 181-0015, Japan*

in original form 2014 October 31

ABSTRACT

We report the discovery of an extremely dense group of massive galaxies at the centre of the protocluster at $z = 3.09$ in the SSA22 field from near-infrared spectroscopy conducted with the Multi-Object InfraRed Camera and Spectrograph (MOIRCS) equipped on the Subaru Telescope. The newly discovered group comprises seven galaxies confirmed at $z_{\text{spec}} \approx 3.09$ within 180 kpc including five massive objects with the stellar masses larger than $10^{10.5} M_{\odot}$ and is associated with a bright sub-mm source SSA22-AzTEC14. The dynamical mass of the group estimated from the line-of-sight velocity dispersion of the members is $M_{\text{dyn}} \sim 1.6 \pm 0.3 \times 10^{13} M_{\odot}$. Such a dense group is expected to be very rare at high redshift as we found only a few comparable systems in large-volume cosmological simulations. Such rare groups in the simulations are hosted in collapsed halos with $M_{\text{vir}} = 10^{13.4} - 10^{14.0} M_{\odot}$ and evolve into the brightest cluster galaxies (BCGs) of the most massive clusters at present. The observed AzTEC14 group at $z = 3.09$ is therefore very likely to be a proto-BCG in the multiple merger phase. The observed total stellar mass of the group is $5.8_{-2.0}^{+5.1} \times 10^{11} M_{\odot}$. It suggests that over half the stellar mass of its descendant had been formed by $z = 3$. Moreover, we identified over two members for each of the four Ly α blobs (LABs) using our new spectroscopic data. This verifies our previous argument that many of the LABs in the SSA22 protocluster associated with multiple developed stellar components.

Key words: galaxies: formation — galaxies: evolution — galaxies: distances and redshifts — galaxies: clusters: general

1 INTRODUCTION

It is still an important open question to understand the early formation history of massive elliptical galaxies. Dissipationless or ‘dry’ equal-mass merger is favored to explain dynamically hot slow-rotating structure of massive systems while segregation of baryon and dark matter in the central part and large phase-space density requires dissipational collapse (e.g., Naab, Khochfar, & Burkert 2006). Significant size and stellar density evolution from high redshift (e.g., Daddi et al. 2005; Trujillo et al. 2007; van Dokkum et al.

2008; van der Wel et al. 2014) may be explained by dry minor mergers which ‘puff-up’ the galaxy structure to be consistent with those observed at present (e.g., Bezanson et al. 2009; Naab, Johansson, & Ostriker 2009; Hopkins et al. 2009). Processes of the formation of massive ellipticals should be also explained in the context of the Λ CDM hierarchical structure growth.

One attractive scenario is the ‘two-phase’ hierarchical multiple mergers that was suggested from modern hydrodynamical cosmological simulations with very high resolution (e.g., Meza et al. 2003; Naab et al. 2007; Oser et al. 2010). In these models, in-situ rapid gas accretion and violent star formation in the first phase is followed by the secondary

* E-mail: marikubo@icrr.u-tokyo.ac.jp

phase of multiple dry minor or major mergers of satellites which are formed outside of the virial radius of a central massive object. This scenario explains naturally the rapid and early star formation as well as the size and stellar density evolution of massive ellipticals. Multiple merger may explain many properties of the most massive galaxies, i.e., support by the anisotropic velocity dispersion, smaller ellipticity and boxy shape, and relatively diffuse core.

It has become understood that feedback processes, especially active galactic nucleus (AGN) feedback, play an very important role in the star-formation history of massive ellipticals (e.g., Croton et al. 2006). To avoid the over-cooling problem for massive halos, AGN feedback seems essential. It is then a quite important and interesting question to reveal how super massive black holes (SMBH) are formed in such hierarchical multiple merging phases. If the progenitors of the SMBH of a massive elliptical have already been formed in the components of multiple merger, the orbital decays of multiple BHs may also affect the final core extension of the galaxy (e.g., Begelman, Blandford, & Rees 1980; Volonteri, Haardt, & Madau 2003).

There is, on the other hand, still a significant lack of the observational constraints for such early history of the massive elliptical galaxy formation. In particular, it is not well understood whether such multiple mergers really occurred at high redshift, and if occurred, what are the properties of the progenitors. Herein, we report a discovery or clear identification of an extremely dense group of massive galaxies at $z = 3$ located in the central region of the known most significant protocluster.

In fact, in the recent deep near-infrared (NIR) imaging observations, possible hierarchical multiple merger sites have been reported as the apparent association of massive stellar components in the starburst galaxies at high-redshift. Double (e.g., Tacconi et al. 2006) or multiple (e.g., Tacconi et al. 2008; Viero et al. 2012) sources are frequently associated with sub-mm galaxies (SMGs). Many of the extended Ly α blobs (LABs) also seem to host more than two stellar systems (Uchimoto et al. 2012; Prescott et al. 2012; Overzier et al. 2013; Yang et al. 2014). In the local Universe, multiple cores which can be the remnants of multiple mergers are sometimes found in the brightest cluster galaxies (BCGs) (e.g., Lauer 1988; Yamada et al. 2002; Laine et al. 2003; Seigar, Lynam, & Chorney 2003).

In order to prove the multiple merging events, however, it is needed to spectroscopically identify the components and to examine their dynamical properties. Here we report the identification of such dense groups by the NIR spectroscopic observations for a sub-mm source, SSA22-AzTEC14 (Tamura et al. 2009; Umehata et al. 2014), as well as the LABs in the core of the SSA22 protocluster at $z = 3.09$. While the SSA22 protocluster is known as the prominent and the most significant density peak of Lyman Break galaxies (LBGs) (Steidel et al. 1998, 2000) and Ly α emitters (LAEs) (Steidel et al. 2000; Hayashino et al. 2004; Yamada et al. 2012), significant overdensities of SMGs (Tamura et al. 2009) as well as LABs (Matsuda et al. 2004, 2011) have also been reported. In our previous photometric study, it was found that some SMGs as well as approximately 40% of the LABs in this protocluster have over two stellar counterparts with $K < 24$ with photometric redshift $z_{\text{phot}} \sim 3.1$ (Uchimoto et al. 2012).

We summarise the selection and observations of the targets in Section 2. In Section 3, we describe the results of the NIR spectroscopic observations and the obtained dynamical properties of the systems. Then, we discuss their properties by comparing them with similar systems in the Millennium simulation (Springel et al. 2005) in Section 4. In Appendix, we give the SED fits of the all galaxies confirmed as the members of the galaxy groups studied here. In this paper, cosmological parameters of $H_0 = 70 \text{ km s}^{-1} \text{ Mpc}^{-1}$, $\Omega_m = 0.3$ and $\Omega_\Lambda = 0.7$ are assumed. The AB magnitude system is used throughout this paper.

2 SELECTION AND OBSERVATIONS OF THE MULTIPLE MERGER CANDIDATES

The targets are the counterparts of a SMG and LABs in the SSA22 protocluster at $z = 3.09$, which were selected in our own deep K_s -band images obtained with the multi-object infrared camera and spectrograph (MOIRCS) equipped on the Subaru Telescope. The details of the dataset and reduction procedures are given in Uchimoto et al. (2012) and Kubo et al. (2013). Briefly, we selected sources with $K < 24$ (5σ detection limit) and $2.6 < z_{\text{phot}} < 3.6$ as candidate protocluster galaxies. In addition, distant red galaxies (DRGs; $J - K > 1.4$, Franx et al. 2003) were selected as the candidate protocluster galaxies. The photometric redshifts of the galaxies were estimated from spectral energy distribution (SED) fitting of their fluxes at $u^*BVRI'z'JHK$, 3.6, 4.5, 5.8 and 8.0 μm -bands (taken by Hayashino et al. 2004; Matsuda et al. 2004; Webb et al. 2009; Uchimoto et al. 2012) with the stellar population synthesis models of Bruzual & Charlot (2003) through a standard χ^2 minimisation procedure. We adopt the Chabrier Initial Mass Function (IMF) (Chabrier 2003) in this paper and Kubo et al. (2015) (here after K15) while the Salpeter IMF (Salpeter 1955) was used in Uchimoto et al. (2012) and Kubo et al. (2013). Adopting the Chabrier IMF, our sample selection is nearly complete for the galaxies with $M_* \geq 1 \times 10^{10} M_\odot$ at $z \sim 3$ if the sample is dominated by normal star forming galaxies. However, as we describe in §3, our sample is biased to rare dusty and/or passively evolving galaxies which have larger stellar mass to light ratios than those of normal star forming galaxies. Therefore we take the conservative stellar mass limit based on the observed stellar populations of the galaxies in each galaxy group in later.

It was reported in Uchimoto et al. (2012) that 40% of the LABs in the SSA22 protocluster have over two K -band counterparts with $2.6 < z_{\text{phot}} < 3.6$ within their Ly α nebulae. They also reported the overdensities of hyper extremely red objects (HEROs; $J - K > 2.1$, Totani et al. 2001) around the AzTEC/ASTE 1.1 mm sources in the SSA22 field (Tamura et al. 2009). The most extreme cases among them are LAB01, LAB02, the largest LABs, and SSA22-AzTEC14 (Umehata et al. 2014) which are plausibly associated with more than five counterparts within the spatial extents of ≈ 150 kpc (Uchimoto et al. 2012, note that the source ID of AzTEC14 was redefined from AzTEC20).

We then conducted NIR spectroscopic observations to confirm the redshifts of the candidate protocluster galaxies. Since Ly α is a resonance line, other nebulae emission lines are more suitable for obtaining the systemic redshifts of the

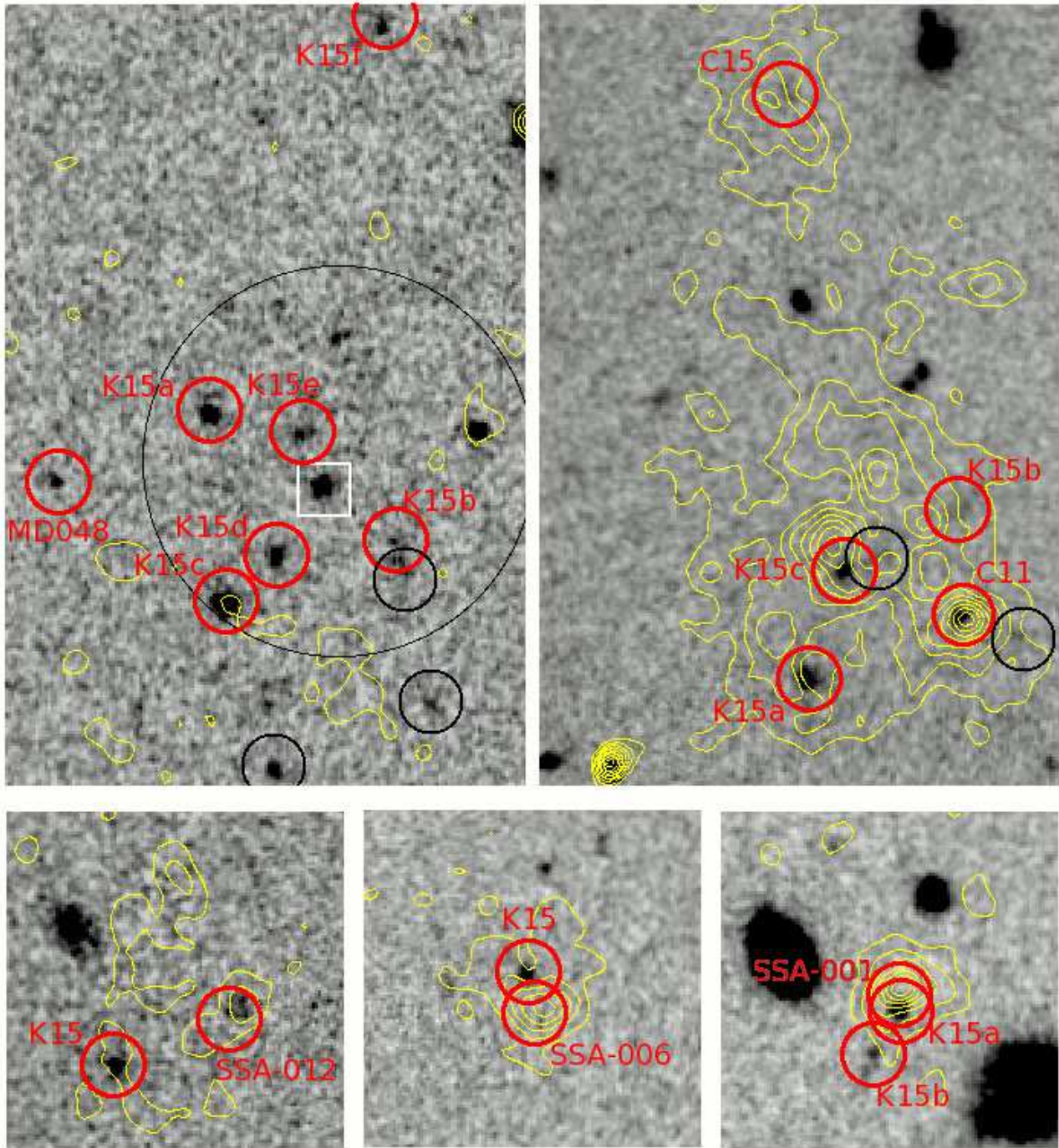


Figure 1. The K_s -band images of the AzTEC14 group (*top left*), LAB01 (*top right*), LAB12 (*bottom left*), LAB16 (*bottom centre*) and LAB30 (*bottom right*). The sizes of the images are 20.0×30.0 arcsec (≈ 150 kpc \times 230 kpc in physical) for the AzTEC14 group and LAB01, and 13.0×13.0 arcsec for LAB12, LAB16 and LAB30. The thick red circles with IDs show the objects with $z_{\text{spec}} = 3.07 - 3.10$. Their IDs correspond to those in Table 1. The black circles indicate the galaxies with $2.6 < z_{\text{phot}} < 3.6$. The white square shows the foreground object with $z_{\text{spec}} = 0.5763$ (K15). The yellow contours show Ly α isophotal area obtained with the BV -band and $NB497$ -band images taken with the Subaru Suprime-Cam (Matsuda et al. 2004) while the coordinates on the K_s -band images were calibrated to those on the Suprime-Cam images. The black large circle on the AzTEC14 group shows the beam-size of the ASTE/AzTEC 1.1 mm source (Umehata et al. 2014).

Table 1. The list of the members of the AzTEC14 group and LABs

Object	R.A. (J2000.0)	Dec (J2000.0)	K_{tot} (mag)	$J - K$ (mag)	M_* ($10^{10} M_{\odot}$)	z_{spec}	Exptime ^a (ks)	Ref ^b
AzTEC 14 group								
Az14-K15a	22:17:37.3	+00:18:23.2	22.5	2.8	$8.0^{+5.7}_{-2.9}$	3.0851 ± 0.0001 3.0926 ± 0.0003	13.6	K15
Az14-K15b	22:17:36.8	+00:18:18.2	23.1	1.6	$9.3^{+19.7}_{-5.0}$	3.0854 ± 0.0003	13.6	K15
Az14-K15c	22:17:37.3	+00:18:16.0	21.6	2.8	$25.4^{+7.3}_{-5.8}$	2.7, 3.0 – 3.15 ^c	13.0	K15
Az14-K15d	22:17:37.1	+00:18:17.9	23.3	1.1	$5.3^{+5.7}_{-2.9}$	3.0774 ± 0.0003	20.0	this study
Az14-K15e	22:17:37.1	+00:18:22.4	23.4	2.0	$7.2^{+9.8}_{-5.2}$	3.0925 ± 0.0002	20.0	this study
Az14-K15f	22:17:36.9	+00:18:38.0	23.1	2.3	$1.7^{+2.2}_{-0.8}$	3.0866 ± 0.0002	20.0	this study
MD048	22:17:37.7	+00:18:20.6	24.1	...	$1.1^{+1.1}_{-0.7}$	3.086	...	S03
LAB01								
LAB01-K15a	22:17:26.1	+00:12:32.3	22.1	1.3	$9.5^{+7.5}_{-2.5}$	3.1000 ± 0.0003	14.0	K15
LAB01-K15b	22:17:25.7	+00:12:38.7	23.6	0.3	$1.1^{+0.6}_{-0.5}$	3.1007 ± 0.0002 ;	14.0	K15
LAB01-K15c	22:17:26.0	+00:12:36.4	22.9	1.4	$8.1^{+2.9}_{-2.4}$	3.099	7.6	W10
C11	22:17:25.7	+00:12:34.7	23.2	1.3	$1.1^{+2.1}_{-0.3}$	3.0999 ± 0.0003	...	M13
C15	22:17:26.2	+00:12:54.7	3.0986 ± 0.0003	...	M13
LAB12								
LAB12-K15	22:17:32.0	+00:16:55.5	22.2	2.6	$11.5^{+23.9}_{-4.9}$	3.0909 ± 0.0004	13.6	K15
SSA22-012	22:17:31.714	+00:16:57.262	23.3	1.2	$2.0^{+2.3}_{-1.1}$	3.0902	...	E14
LAB16								
LAB16-K15	22:17:24.85	+00:11:17.60	23.1	0.8	$4.1^{+3.0}_{-2.0}$	3.0689 ± 0.0002	14.0	K15
SSA22-006	22:17:24.833	+00:11:16.002	>25.2	3.0691	...	E14
LAB30								
LAB30-K15a	22:17:32.45	+00:11:32.87	23.0	0.9	$4.2^{+0.2}_{-0.6}$	3.0687 ± 0.0004	14.0	K15
LAB30-K15b	22:17:32.52	+00:11:31.22	23.4	0.4	$4.4^{+0.2}_{-0.3}$	3.0680 ± 0.0003	14.0	K15
SSA22-001 ^d	22:17:32.453	+00:11:33.513	3.0690	...	E14

^a Exposure times of our NIR spectroscopic observations

^b The reference of the redshifts are Steidel et al. (2003) (S03), Weijmans et al. (2010) (W10), McLinden et al. (2013) (M13), Erb et al. (2014) (E14) and Kubo et al. (2015) (K15). The redshifts cited from S03 and W10 were obtained with the optical spectroscopy while others were obtained with the NIR spectroscopy.

^c There is a large uncertainty since the redshift of this object was measured with the Balmer/4000 Å breaks of its stacked continuum spectrum.

^d This object is likely to be the same as LAB30-K15a

stellar components associated with LABs. For galaxies at $z \approx 3.09$, [OIII] $\lambda 5007$ emission line is the strongest observable emission line in the NIR. The observations were conducted with MOIRCS in September and October 2012 (K15) and in June and July 2014. We observed the counterparts of SSA22-AzTEC14 and LAB01 intensively. In addition to these unique objects, LAB12, LAB16 and LAB30 were observed. The details of the observations and data reduction procedures, and the complete list of our NIR spectroscopic sample in the 2012 run are given in K15. To summarise, the detection limit of the data taken in the 2012 run was $\sim 1 - 2 \times 10^{-17} \text{ erg s}^{-1} \text{ cm}^{-2}$ ($\sim 3\sigma$ of the background at $\sim 2.05 \mu\text{m}$) when the exposure time was 13.0 – 14.0 ks for each mask. During the observation in June 2014, the full width at half maximum (FWHM) of the point spread function (PSF) ranged from 0.35 to 0.4 arcsec. The total exposure time was 20.0 ks for this mask. Consequently, emission

lines as faint as $6.5 \times 10^{-18} \text{ erg s}^{-1} \text{ cm}^{-2}$ were detected. On the other hand, in July 2014, humidity was high and the FWHM of the PSF during the observation ranged from 0.5 to 0.8 arcsec. Owing to the poor conditions and short exposure time of 7.6 ks, the limiting flux value of the taken in that run was $\sim 2 - 3 \times 10^{-17} \text{ erg s}^{-1} \text{ cm}^{-2}$, which was too shallow to detect the redshifted [OIII] $\lambda 5007$ emission lines of the galaxies at $z \sim 3$ at most.

3 RESULTS

3.1 Spectroscopic redshifts

We summarise the spectroscopic redshifts of the SMG and LABs studied here in Table 1. The redshifts and flux values of the [OIII] $\lambda 5007$ emission lines of the newly confirmed counterparts are listed in Table 2. We measure the

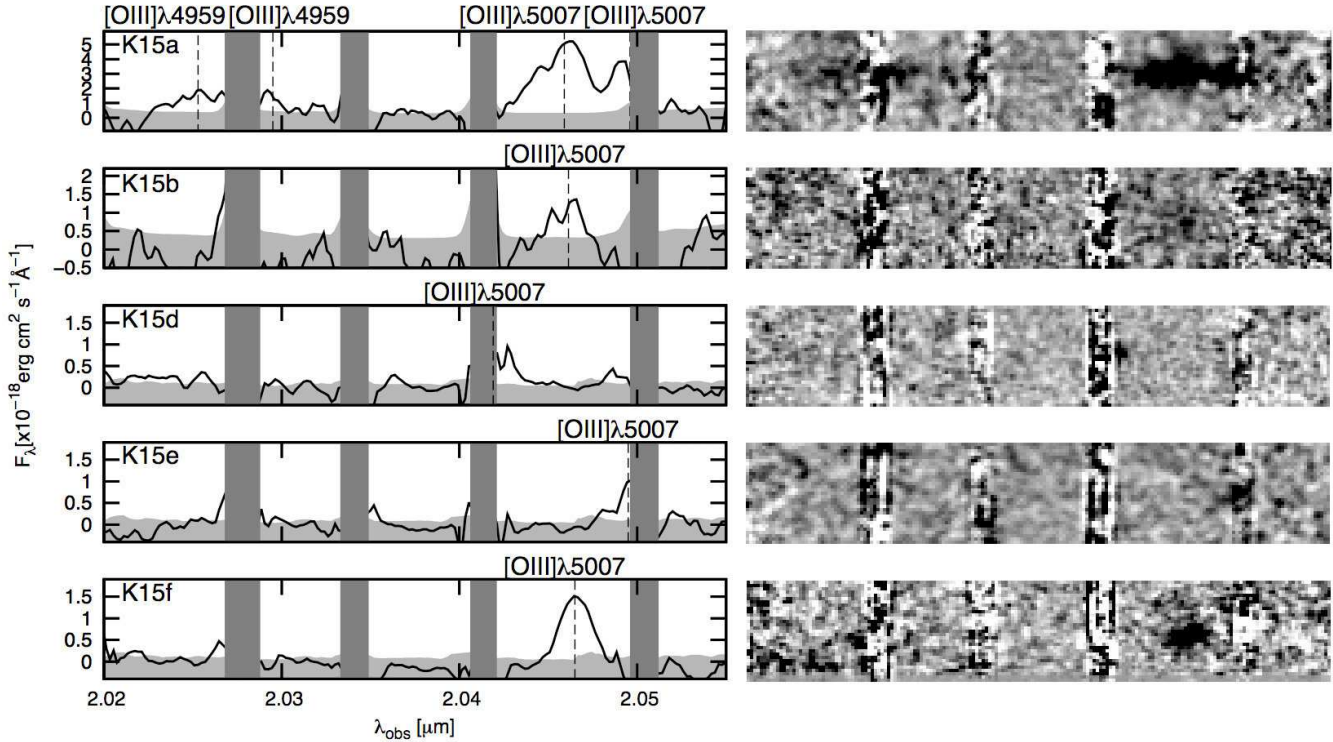


Figure 2. Left panels: The solid lines show the one-dimensional spectra of Az14-K15a, b, d, e and f at 2.020 to 2.055 μm from top to bottom. The dashed vertical lines indicate the centres of the detected emission lines. Only the [OIII] $\lambda 5007$ emission lines are detected at most while the [OIII] $\lambda 4959$ are also detected for Az14-K15a. The grey shaded regions show the 1σ background noise at each point. Dark grey areas mask the regions buried in strong OH sky emission lines. Right panels: The images of the spectra correspond to the left panels.

Table 2. The list of the newly confirmed counterparts of the AzTEC14 group

Object	$z_{[\text{OIII}]}$	$F_{[\text{OIII}]\lambda 5007}$ (10^{-17} erg/s/cm 2)
Az14-K15d	3.0774 ± 0.0003	2.2 ± 0.2
Az14-K15e	3.0925 ± 0.0002	1.5 ± 0.1
Az14-K15f	3.0866 ± 0.0002	3.2 ± 0.4

redshifts and flux values by fitting the emission lines with the Gaussian functions. Although only one emission line was detected for most of the targets, the photometric redshifts suggest that they are [OIII] $\lambda 5007$ at $z \sim 3.09$. Fig. 2 shows the spectra of the counterparts of SSA22-AzTEC14. About half the emission lines of Az14-K15d and -K15e are likely hidden by OH sky emission lines. Their redshifts are estimated by fitting their line profiles taking the hidden regions into account. Besides our own redshifts, we cite the spectroscopic redshifts from Steidel et al. (2003), Weijmans et al. (2010), McLinden et al. (2013) and Erb et al. (2014). Here we treat the spectroscopically confirmed counterparts as the group members. Two or more galaxies are confirmed for the counterparts of SSA22-AzTEC14 (hereafter referred to the AzTEC14 group), LAB01, LAB12, LAB16 and LAB30.

The stellar mass values of the galaxies are estimated from the SED fitting with the same procedure as that in K15. Before the fitting, we subtracted the [OIII] $\lambda 5007$ emission-line contribution from the K -band magnitude, which results in a correction

of < 0.1 mag. The observed and best-fit SEDs of all the counterparts are shown in the Appendix. Az14-K15a and LAB12-K15 are the AGNs detected in X-ray (Lehmer et al. 2009) but they have no significant AGN feature in their SEDs and are well fitted with the SED models of galaxies. The errors of the stellar masses show a 68% confidence level in the probability distribution for the stellar masses calculated from a minimum χ^2 value for each object. The uncertainties in the redshifts have only negligible effects on those in the SED fits and stellar masses. Assuming that the typical stellar population of the galaxies in each group is given by those of the confirmed counterparts, the completeness may decline substantially for galaxies with $M_* \leq 4 \times 10^{10} M_\odot$ and $M_* \leq 2 - 3 \times 10^{10} M_\odot$ in the AzTEC14 group and the LABs, respectively.

Fig. 1 shows the MOIRCS K_s -band images of the AzTEC14 group and the LABs. The yellow contours show the isophotal areas of Ly α emission at $z = 3.09$, which was drawn from the NB497-band images subtracted with the BV -band images both obtained using the Subaru Suprime-Cam (Matsuda et al. 2004). The objects whose redshifts were confirmed in other studies sometimes show no significant K_s -band counterpart while they are identified as i.e., LBGs or the surface brightness peaks of Ly α nebulae. Surface number densities of the galaxies with $K < 24$ at $z_{\text{spec}} \approx 3.09$ are 232 arcmin^{-2} for the AzTEC14 group excluding Az14-K15f (60 arcmin^{-2} , if we include Az14-K15f) and 132 arcmin^{-2} for LAB01, estimated by taking the aperture areas containing all the group members with $K < 24$. These surface number densities are 60 and 30 times larger than those in the central part of the SSA22 protocluster studied with MOIRCS, which is 1.7 times larger than that in the blank field (Kubo et al. 2013). Such a dense group of physically associated massive galaxies has

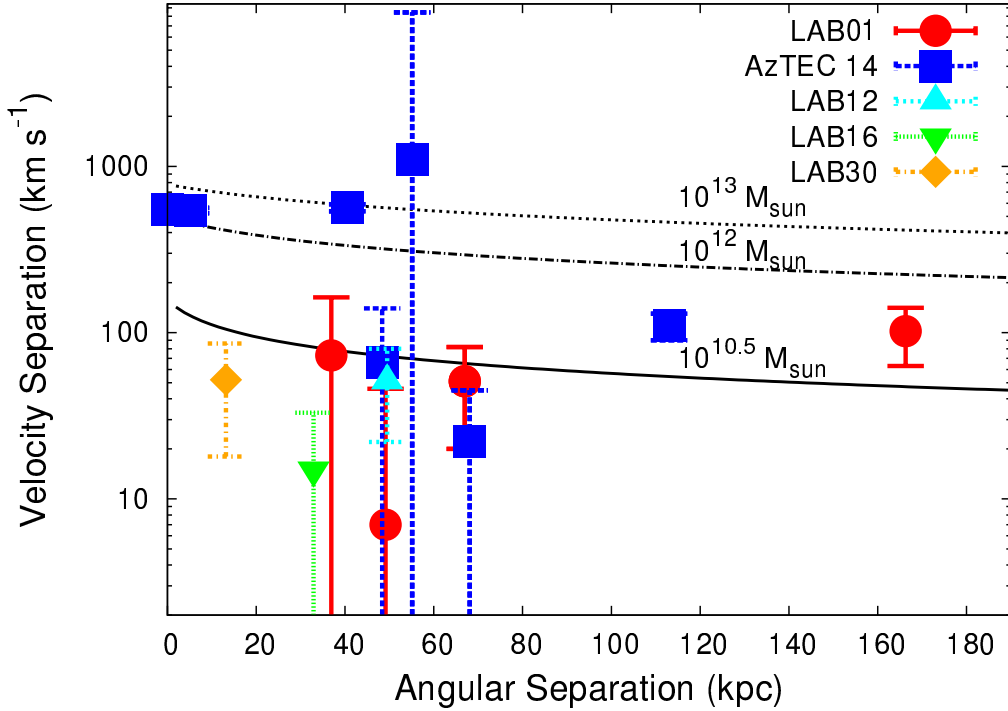


Figure 3. The line-of-sight velocity and spatial distributions of the group members. Blue squares, red circles, a cyan triangle, a green reversed triangle and an orange diamond show angular spatial separations and line-of-sight velocity offsets of the counterparts from the central counterparts of the AzTEC14 group, LAB01, LAB12, LAB16 and LAB30, respectively. The solid, dashed dotted and dotted curves indicate the escape velocities from the objects with $M_{\text{halo}} = 10^{10.5}$, 10^{12} and $10^{13} M_{\odot}$, respectively, calculated assuming the Navarro-Frenk-White (NFW; Navarro, Frenk, & White 1997) mass profile. We assume the concentration parameter $c = 5$ for the halo with $M_{\text{halo}} = 10^{13} M_{\odot}$, and $c = 4.5$ for the halos with $M_{\text{halo}} = 10^{10.5}$ and $10^{12} M_{\odot}$ predicted in Klypin, Trujillo-Gomez, & Primack (2011).

never been confirmed at $z > 3$. Similarly MacKenzie et al. (2014) found a plausible lensed compact group of galaxies at $z \sim 2.9$ but based on a photometric lensing model.

The following describes the properties of the individual objects studied here. In this paper, we do not refer the total star formation rates (SFRs) of the groups estimated from the SED fitting since there are large uncertainties due to the faint counterparts.

3.1.1 The AzTEC14 group

In addition to K15, we newly confirmed three counterparts. The redshifts and flux values of the [OIII] $\lambda 5007$ emission lines of the newly confirmed counterparts are listed in Table 2. In total, seven galaxies at $z_{\text{spec}} \approx 3.09$ were confirmed. Note that there is a large redshift uncertainty for Az14-K15c since its redshift was measured with the Balmer/4000 Å breaks of its stacked continuum spectrum but here we treat this object as a very plausible member of the group. Fig. 2 shows the spectra of the members of the AzTEC14 group. Az14-K15a shows the extended emission lines with double peaks which can be originated in a dual AGN and/or the gas motion in the narrow line region of an AGN; this object is an AGN detected in X-ray (Lehmer et al. 2009).

The members of the AzTEC14 group are dominated by extremely red objects classified as DRGs and HEROs (Uchimoto et al. 2012). Some of them are dusty red galaxies since they are plausible counterparts of an 1.1 mm source and an IRAM PdBI source is certainly identified at the location of Az14-K15e (Umehata et al. in prep). On the other hand,

there are also some old red galaxies like Az14-K15a and Az14-K15c which are well characterized as massive quiescent galaxies in K15. The total SFR estimated from the flux values of the [OIII] $\lambda 5007$ emission lines is $85.1 \pm 8.7 M_{\odot} \text{ yr}^{-1}$, adopting $\text{SFR}_{\text{H}\alpha} (M_{\odot} \text{ yr}^{-1}) = L(\text{H}\alpha) / 1.12 \times 10^{41} \text{ ergs s}^{-1}$ (Kennicutt 1983) and assuming that the [OIII] $\lambda 5007$ to H α ratio is unity, where the no reddened H α /H β ratio is 2.88 (Osterbrock 1989) and [OIII]/H β ratios are empirically $\sim 0.3 - 30$ for $z = 2 - 3$ star forming galaxies (e.g., Steidel et al. 2014). Here, the extinction of and the contribution of AGNs to the [OIII] $\lambda 5007$ emission lines are ignored.

3.1.2 LAB01

In total, four galaxies were confirmed as the counterparts of LAB01. The redshifts of LAB01-K15a, b and C11 were determined from the [OIII] $\lambda 5007$ emission lines. For LAB01-K15c, we use $z_G = 3.099$ obtained by Weijmans et al. (2010) as the systemic redshift, which was measured by fitting the Ly α line profile with Gaussian plus absorption features of the spectrum of the optical source detected at the position of LAB01-K15c (R3 in Weijmans et al. 2010). We conducted the NIR spectroscopy of this object in July 2014 but failed to detect any emission line probably due to the poor condition. C15 within the north nebula of LAB01 was also confirmed at the redshift close to those of the counterparts of LAB01. The redshifts were also measured with Ly α for LAB01-C11 and C15, which offset from the systemic redshifts measured with [OIII] $\lambda 5007$ by -51.3 ± 42.1 and $+5.8 \pm 32.9$

km s⁻¹, respectively (McLinden et al. 2013). These offsets are lower than those of typical LAEs (~ 200 km s⁻¹ Erb et al. 2014).

SFR_[OIII] of LAB01 is $64.6 \pm 6.5 M_{\odot} \text{ yr}^{-1}$ in total. Note that there may be dust obscured star formation activities and/or QSOs since LAB01-K15a and LAB01-K15c are detected in *Spitzer* MIPS 24 μm (Webb et al. 2009) and JCMT/SCUBA-2 850 μm (Geach et al. 2014).

3.1.3 LAB12, LAB16 and LAB30

The redshifts of the counterparts for LAB12, LAB16 and LAB30 in Table 1 were determined from the [OIII] $\lambda 5007$ emission lines. The redshifts measured with Ly α offset from the systemic redshifts measured with [OIII] $\lambda 5007$ by $+278 \pm 50$ km s⁻¹, $+508 \pm 68$ km s⁻¹ and $+442 \pm 19$ km s⁻¹ for LAB12-S012, LAB16-S006 and LAB30-S001, respectively (Erb et al. 2014), which are similar to those of the typical LBGs.

The total SFR_[OIII] of LAB12, LAB16 and LAB30 are 9.4 ± 1.9 , 18.1 ± 1.2 and $5.8 \pm 1.4 M_{\odot} \text{ yr}^{-1}$, respectively. LAB12-K15 is characterized as a massive quiescent galaxy with an AGN (K15).

3.2 Velocity distributions on the groups

Fig. 3 shows the angular spatial separations and line-of-sight velocity offsets of the group members from their centres, where the centre of a group is defined as the location and redshift of the group member with the largest stellar mass. We treat Az14-K15a as the centre of the AzTEC14 group since the redshift uncertainty of Az14-K15c is large. Nonetheless, its redshift is close to the median redshift of the AzTEC14 group.

The solid, dashed dotted and dotted curves in Fig. 3 indicate the escape velocities from the halos with halo mass $M_h = 10^{10.5}$, 10^{12} and $10^{13} M_{\odot}$, respectively, calculated assuming the Navarro-Frenk-White (NFW; Navarro, Frenk, & White 1997) mass profile with the concentration parameter $c = 5$ for $M_h = 10^{13} M_{\odot}$, and $c = 4.5$ for $M_h = 10^{10.5} M_{\odot}$ and $10^{12} M_{\odot}$. We assume the concentration parameters at $z \sim 3$ predicted in Klypin, Trujillo-Gomez, & Primack (2011). Note that here we ignore the line-of-sight separations and the velocities in the transverse direction. The objects below these curves can be dynamically bound to one system with these mass values. The AzTEC14 group can be bound to an object with mass larger than $10^{13} M_{\odot}$. Assuming that the AzTEC14 group is spherical symmetry and in the dynamical equilibrium, its dynamical mass is estimated to be $M_{\text{dyn}} = 3\sigma_v^2 R/G \sim 1.6 \pm 0.3 \times 10^{13} M_{\odot}$, where the velocity dispersion of the members σ_v is 365 ± 34 km s⁻¹ and the spatial extent R is ≈ 180 kpc. Similarly, the LABs can be bound to objects with mass $\gtrsim 10^{10.5} M_{\odot}$, although it is lower than the total stellar masses of the LABs of $M_* = 0.4 \sim 2.0 \times 10^{11} M_{\odot}$.

4 DISCUSSION

4.1 Mass constraints of the groups

The observed velocity distributions of the group members show only a part of their dynamical properties. First, the observed velocities and spatial distributions of the galaxies are the projected ones. Second, the groups probably represent the properties of only the central parts of their host halos.

To evaluate the physical properties of the groups, we compare our samples with the galaxy groups selected from the galaxy formation models based on the Millennium simulation (Springel et al. 2005). We assume that the observed groups represent the central dense parts of virialised halos. We select the comparison groups which contain the same number of galaxies with the stellar mass larger than the completeness limit as our sample

groups from the groups hosted within the collapsed halos at $z \sim 3$ (at the $z = 2.86$ and $z = 3.06$ snapshots) in a comoving volume of $1.25 \times 10^8 h^{-3} \text{ Mpc}^3$ of the full Millennium simulation. The comparison Millennium groups are also within the same angular sizes as our sample groups. For example, a group containing five galaxies with $M_* \geq 4 \times 10^{10} M_{\odot}$ within 120 kpc from their centre is selected as the comparison group for the AzTEC14 group. We use the galaxy catalogues based on the galaxy formation models of De Lucia & Blaizot (2007) and Guo et al. (2011). In the latter model, the efficiency of galaxy formation, especially in low mass halos decreases to fit the observed values. The Chabrier IMF is adopted in both the galaxy formation models.

Fig. 4 shows the comparisons of the spatial and velocity distributions of our samples and the comparison Millennium groups at $z \sim 3$ selected from Guo et al. (2011). Light grey points show the physical spatial and velocity separations of the members of the comparison Millennium groups, and dark grey points with the same symbols show those seen from one direction. We show the mean physical spatial separations expected from their angular separations, namely the angular separations multiplied by $\pi/2$, and the mean velocity offsets seen from one direction expected from their physical velocity separations, i.e. the physical velocity separations multiplied by $4/\pi^2$. Note that for the AzTEC14 group, only one comparison group is found in each $z \sim 3$ snapshot of the full Millennium volume and such groups are only found at the centres of collapsed massive halos. It is because, as we describe later, massive halos which can host AzTEC14-like groups are very rare at $z \sim 3$. The velocity distributions of the AzTEC14 group and LAB30 closely resemble to those of the projected comparison Millennium groups. On the other hand, the velocities of the galaxies associated with LAB01 are on average lower than those in the comparison Millennium groups. This suggests that LAB01 is actually hosted in a lower mass halo or associated with the galaxies which are dynamically bound but just falling into the potential of the central high density region.

Fig. 5 shows the stellar mass distributions of the AzTEC14 group, LAB01 and their comparison groups in De Lucia & Blaizot (2007) and Guo et al. (2011). The observed stellar mass distributions agree well with both the Millennium models at above the completeness limit. Indeed, the comparison of our groups and the Millennium groups is reasonable at above this limit, although there can be further differences at low mass galaxies. As e.g., Quilis & Trujillo (2012) reported, the numbers of satellite galaxies around the local massive galaxies are smaller than those predicted by the galaxy formation models based on the Millennium simulation.

We now consider the masses of the halos which host such multiple massive galaxies. At each $z \sim 3$ snapshot of the Millennium simulation, only one massive halo hosts the comparison group of the AzTEC14 group; The halos with the virial mass $M_{\text{vir}} \approx 10^{13.9}(10^{14.0}) M_{\odot}$ and $10^{13.9}(10^{13.6}) M_{\odot}$ at the $z = 3.06$ (or at the $z = 2.86$) snapshot respectively host the comparison groups in the De Lucia & Blaizot (2007) and Guo et al. (2011) models. In the De Lucia & Blaizot (2007) model, the comparison Millennium group of the AzTEC14 group at $z = 2.86$ is the descendant of the comparison group at $z = 3.06$. In the Guo et al. (2011) model, another massive halo happens to host the comparison group of the AzTEC14 group at $z = 2.86$ while the number of the galaxies in the descendant of the comparison group at $z = 3.06$ decreases by mergers. Since the comparison groups of the AzTEC14 group are very rare at $z \sim 3$, we also see the halo mass distribution of such groups by rescaling the galaxy groups at low redshift to be at $z = 3$. We select the galaxy groups which contain the same numbers of galaxies within the same angular sizes as the AzTEC14 group in the comoving scale from the $z = 0 - 0.5$ snapshots of the Millennium simulation, assuming that the virial masses of the halos are preserved but their sizes evolve as $\propto (1+z)^{-1}$. The local comparison groups of the

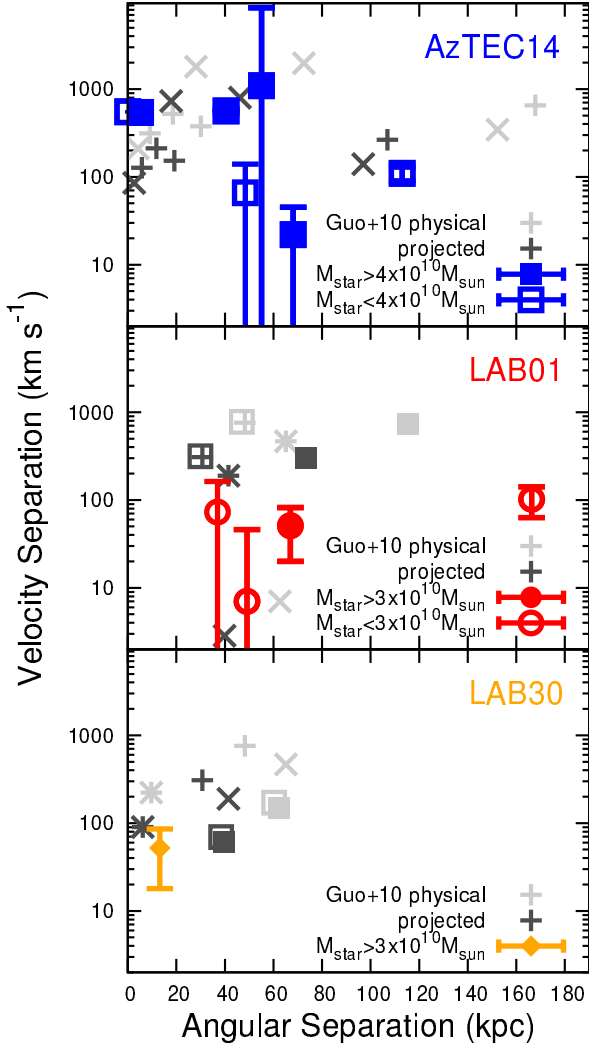


Figure 4. The comparison of the velocity and spatial distributions of our samples and the galaxy groups selected from the galaxy formation models based on the Millennium simulation. Top panel: Blue filled and blank squares show the members of the AzTEC14 group with $M_* \geq 4 \times 10^{10} M_\odot$ and $M_* < 4 \times 10^{10} M_\odot$, respectively. Light grey cross and x-mark points show the physical separations and velocity distributions of the galaxies with $M_* \geq 4 \times 10^{10} M_\odot$ in the comparison Millennium groups selected from the $z = 2.86$ and $z = 3.06$ snapshots of Guo et al. (2011), respectively. Dark grey points shown with the same symbols as the light grey points show the physical separations and velocity distributions seen from one direction. Middle panel: Similar to the top panel but red filled and blank circles show the counterparts of LAB01 with $M_* \geq 3 \times 10^{10} M_\odot$ and $M_* < 3 \times 10^{10} M_\odot$, respectively. Light grey and dark grey points are similar to those in the top panel but for the galaxies with $M_* \geq 3 \times 10^{10} M_\odot$ in the comparison Millennium groups selected from the $z = 3.06$ snapshot. Bottom panel: Similar to the middle panel but for LAB30 shown with an orange diamond.

AzTEC14 group are also hosted in very massive halos while their host halo masses range from $M_{\text{vir}} = 10^{13.7}$ to $10^{14.0} M_\odot$ with median $10^{13.9} M_\odot$ for the De Lucia & Blaizot (2007) model and from $M_{\text{vir}} = 10^{13.6}$ to $10^{14.2} M_\odot$ with median $10^{13.9} M_\odot$ for the Guo et al. (2011) model.

Conversely, LAB01 and LAB30 host two galaxies with $M_* \geq 3 \times 10^{10} M_\odot$ within 80 kpc and 60 kpc, respectively. The masses of the Millennium halos hosting the comparison groups at $z = 3.06$ range from $M_{\text{vir}} = 10^{12.2}$ to $10^{14.0} M_\odot$ with median $10^{13.2} M_\odot$ for the De Lucia & Blaizot (2007) model and from $M_{\text{vir}} = 10^{12.4}$ to $10^{14.1} M_\odot$ with median $10^{13.2} M_\odot$ for the Guo et al. (2011) model. These are similar to those of the host halos of the comparison groups selected at low redshift with rescaling.

From these results, we argue that the groups found in the SSA22 protocluster match well with the groups hosted in massive halos at $z \sim 3$ in the Millennium simulation. By tracing the evolution of a comparison group for the AzTEC14 group from $z \sim 3$, most of its members merge into one massive galaxy at the centre of its host halo while the host halo becomes 10 times massive in the local Universe. This predicts that the AzTEC14 group will evolve into the BCG of one of the most massive clusters in the local Universe, whereas the SSA22 protocluster itself is thought to be a progenitor of one of the most massive clusters (Yamada et al. 2012; K15). The comparison groups of LAB01 and LAB30 at $z \sim 3$ also mostly merge into massive galaxies at $z = 0$.

4.2 Assembly histories of the most massive galaxies

As we discussed above, we are very likely to see multiple merging phases in the formation history of massive galaxies. In this subsection, we discuss their assembly histories.

As mentioned earlier, the most plausible descendant of the AzTEC14 group is a BCG with $M_* \sim 10^{12} M_\odot$ hosted within one of the most massive clusters. Stellar mass of $10^{12} M_\odot$ is a sort of maximum while the stellar mass of a BCG depends on the mass of its host cluster (e.g., Stott et al. 2012). Over half the stellar mass of its descendant is present at $z \sim 3$, when the total stellar mass of the AzTEC14 group is already $M_* = 5.8_{-2.0}^{+5.1} \times 10^{11} M_\odot$. Given that the SEDs of Az14-K15a and Az14-K15c are well characterised as those of the galaxies with burst-like star formation histories and ages of 0.3–2 Gyr (K15), a third of the stellar mass of the descendant of the AzTEC14 group may have been formed by $z \sim 3.6$. On the other hand, the total stellar masses of the LABs range from $M_* = 0.4\text{--}2.0 \times 10^{11} M_\odot$, which are already comparable with over half the stellar masses of massive ellipticals in local clusters. Our results support the early formation of the stars of massive ellipticals in the form of multiple progenitors, as predicted by cosmological numerical simulations (e.g., Meza et al. 2003; Naab et al. 2007; De Lucia & Blaizot 2007; Oser et al. 2010).

The presence of massive quiescent galaxies implicates that some quenching mechanisms must have already been invoked for at least a part of the groups. Large velocity offsets of Ly α from systemic redshifts in some members of LABs indicate the strong outflow. In addition, AGNs are found in the massive quiescent counterparts of LAB12 and the AzTEC14 group, although their AGN activities are only slightly higher than those of massive ellipticals in the local Universe (K15). Moreover, since they are likely to be hosted in massive halos with $M_{\text{halo}} \gtrsim 10^{13} M_\odot$, gravitational heating can globally suppress their star formation activities (e.g., Dekel & Birnboim 2008).

It is also interesting to discuss how SMBHs have grown in the groups. In our sample, LAB12-K15 and AzTEC14-K15a are detected in X-ray with *Chandra* (Lehmer et al. 2009). Moreover, the large line widths of some counterparts suggest the presence of AGNs while the instrumental resolution corrected velocity dispersions estimated from [OIII] $\lambda 5007$ of LAB01-K15a, LAB12-K15

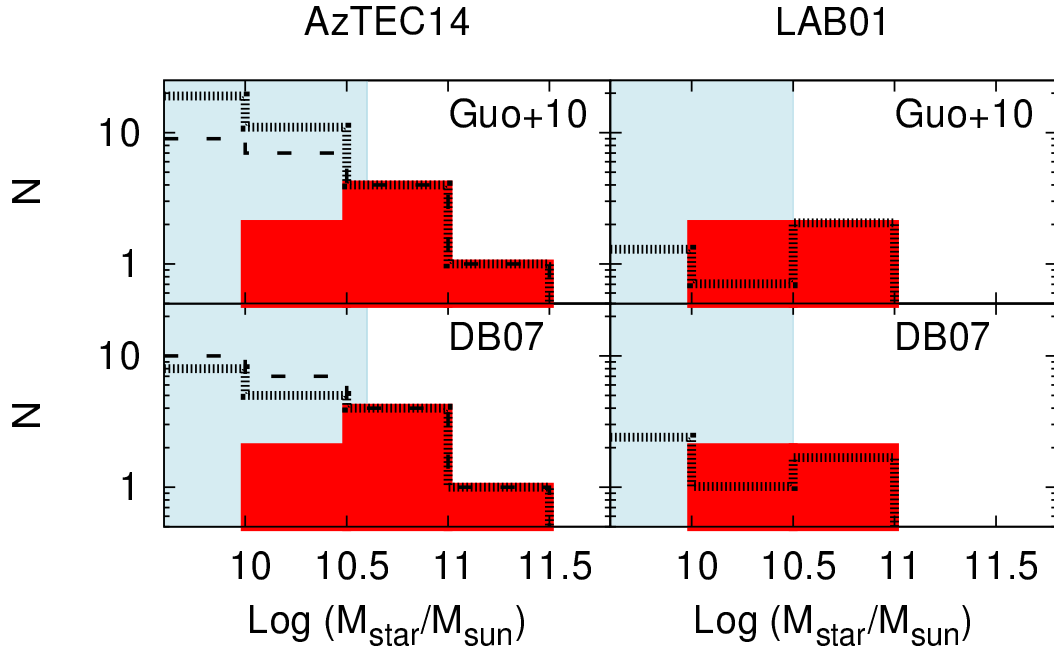


Figure 5. Left top panel: Red filled histogram shows the stellar mass distribution of the AzTEC14 group. The histograms drawn with black dashed and dotted lines are those of the comparison Millennium groups selected from the snapshots at $z = 2.86$ and $z = 3.06$ of the Guo et al. (2011) model, respectively. Grey shaded region indicates the stellar mass range below the completeness limit estimated from the observed stellar populations of the counterparts of the AzTEC14 group. Left bottom panel: Similar to the left top panel but the comparison Millennium groups are selected from the De Lucia & Blaizot (2007) model. Right top panel: Similar to the left top panel but the red histogram shows the stellar mass distribution of LAB01. The histogram drawn with a black dotted line shows the averaged stellar mass distribution of the comparison Millennium groups selected from the $z = 3.06$ snapshot of the Guo et al. (2011) model. Right bottom panel: Similar to the right top panel but the comparison Millennium groups are selected from the De Lucia & Blaizot (2007) model.

and AzTEC14-K15a are $111 \pm 43 \text{ km s}^{-1}$, $139 \pm 19 \text{ km s}^{-1}$, and $225 \pm 11 \text{ km s}^{-1}$ (shorter) and $102 \pm 17 \text{ km s}^{-1}$ (longer), respectively, which are larger than those of the typical galaxies at $z = 2-3$ with similar stellar mass (Erb et al. 2006). Interestingly, the most massive member of the AzTEC14 group, AzTEC14-K15c shows no significant detection in X-ray. X-ray luminosity is given as $L_X = 2 \times 10^{43} (M_{\text{BH}}/10^8 M_{\odot})(\epsilon_X/0.01)(R_{\text{edd}}/0.1) \text{ erg s}^{-1}$ where ϵ_X is the bolometric fraction of the X-ray emission at 2–10 keV and R_{edd} is the Eddington ratio (Yamada et al. 2009). Assuming $M_{\text{BH}}/M_{\text{sph}} \approx 0.002$ of local value, $\epsilon_X = 0.01$ and $R_{\text{edd}} = 0.1$, Az14-K15c can have $L_X \sim 1 \times 10^{44} \text{ erg s}^{-1}$, which is larger than the detection limit of the existing *Chandra* data $\sim 10^{42.6} \text{ erg s}^{-1}$ at 2–8 keV, which suggests that its ϵ_X , R_{edd} and/or $M_{\text{BH}}/M_{\text{sph}}$ ratio are several times lower than the above values. Since AzTEC14-K15c is well characterized as a massive quiescent galaxy, its accretion rate may be low. Therefore subsequent mergers of BHs and/or accretion of matter induced by galaxy mergers may be required to grow its SMBH. Such mergers accompanied with SMBHs are of particular importance that they can heat to reduce the central stellar mass by energy release during the orbital decays of binary SMBHs and reproduce the observed core structures of massive ellipticals (e.g., Begelman, Blandford, & Rees 1980; Volonteri, Haardt, & Madau 2003).

4.3 LABs and SMGs

The origin of LABs is a long argued mystery. Several scenarios have been proposed as the origin of their extended Ly α halos, like hidden QSOs (e.g., Haiman & Rees 2001), obscured star-

burst with strong super-winds induced by death of massive stars (e.g., Taniguchi & Shioya 2000) and release of gravitational energy from cold streams (e.g., Dekel & Birnboim 2008). Our results verify the argument of Uchimoto et al. (2012) that the substantial fraction of the LABs in the SSA22 protocluster are associated with massive stellar components. Interestingly, the locations of the stellar components do not always match with the surface brightness peaks of Ly α . This suggests that some of the Ly α is possibly emitted from and/or scattered by neutral hydrogen gas, and/or ionized by leaked emission from obscured sources.

It is also interesting to compare the properties of the galaxy groups associating with SMGs and LABs. Both objects are plausible progenitors of massive galaxies in multiple merging phases in the SSA22 protocluster. Some LABs in the SSA22 field are significantly detected in the SCUBA 850 μm (Geach et al. 2005) and the AzTEC/ASTE 1.1 mm (Tamura et al. 2013) with the yielded mean 1σ noise limit of $S_{850 \mu\text{m}} = 1.5 \text{ mJy}$ and an rms noise level of $S_{1.1 \text{ mm}} = 0.7 - 1 \text{ mJy beam}^{-1}$, respectively. On the other hand, most of the LABs are not likely to be bright sub-mm sources; It was reported by Tamura et al. (2013) that most of the LABs in the SSA22 field are not significantly detected in the AzTEC/ASTE 1.1 mm survey and their stacked 1.1 mm flux density is $S_{1.1 \text{ mm}} < 0.40 \text{ mJy}$ (3σ).

Both the AzTEC14 group and LAB01 have multiple massive stellar components and large spatial extents but the former shows no significant Ly α emission. LAB01 is associated with an 850 mm source with $S_{850 \mu\text{m}} = (4.6 \pm 1.1) \text{ mJy}$ (Geach et al. 2014) and the 1.1 mm flux density of LAB01 is $1.97 \pm 0.74 \text{ mJy}$ ($S/N=2.7$, Tamura et al. 2013) while that of SSA22-AzTEC14 is $S_{1.1 \text{ mm}} = (5.0 \pm 0.7) \text{ mJy}$ (Umeshata et al. 2014). There are sev-

eral possible scenarios inducing the Ly α deficiency in the group scale. There can be further supply of dust among the AzTEC14 group and LAB12, which has a sparse Ly α nebula, since they host well characterised massive quiescent galaxies as old as the age at which the dust ejections from AGB stars become effective (Sloan et al. 2009). The large velocity dispersion of the AzTEC14 group implies that the dust and gas geometry in the group has been mixed much more by interactions and mergers of galaxies than those in LAB01. Moreover, gravitational heating of a halo can overcome the cooling by filamentary cold streams (Dekel & Birnboim 2008) in the AzTEC14 group. Although it may not be the general case since this group is a very rare massive object at $z \sim 3$. Further studies with ALMA will help us to solve the different nature of the galaxy groups coexisting in such a dense environment.

5 CONCLUSIONS

We discovered a very dense physically associated group of galaxies as the counterparts of a SMG in the SSA22 protocluster at $z = 3.09$ called the AzTEC14 group. By comparing with the galaxy formation models based on the Millennium simulation, we found that the AzTEC14 group shows similar properties as those of the Millennium groups hosted in halos with $M_{\text{vir}} = 10^{13.4} - 10^{14.0} M_{\odot}$ at $z \sim 3$. Most of the members of such a Millennium group at $z \sim 3$ merge into one central massive galaxy at the centre of a halo that is 10 times massive in the current Universe. We also confirmed two or more counterparts of the four LABs. Similarly, they are comparable with the Millennium groups hosted in halos with median mass $M_{\text{vir}} \sim 10^{13.2} M_{\odot}$. The total stellar masses of the AzTEC14 group and the LABs are already larger than about half the stellar masses of BCGs or massive ellipticals in the local Universe, suggesting the early formation of stars in each group. Our results strongly support the hierarchical formation of massive galaxies predicted in the Λ CDM cosmology.

ACKNOWLEDGMENTS

This study is based on data collected at Subaru Telescope, which is operated by the National Astronomical Observatory of Japan. We would like to thank the Subaru Telescope staff for many help and support for the observations. Our studies owe a lot deal to the archival Subaru Suprime-Cam (Matsuda et al. 2004), *Spitzer* IRAC & MIPS data taken in Webb et al. (2009), *Chandra* data taken in Lehmer et al. (2009). We also thank to AzTEC/ASTE observers of the SSA22 field providing the updated source catalog. This work was supported by Global COE Program "Weaving Science Web beyond Particle-Matter Hierarchy", MEXT, Japan. YM acknowledges support from JSPS KAKENHI Grant Number 20647268. This work was partially supported by JSPS Grants-in-Aid for Scientific Research No.26400217.

REFERENCES

- Begelman M. C., Blandford R. D., Rees M. J., 1980, *Natur*, 287, 307
- Bezanson R., van Dokkum P. G., Tal T., Marchesini D., Kriek M., Franx M., Coppi P., 2009, *ApJ*, 697, 1290
- Bruzual G., Charlot S., 2003, *MNRAS*, 344, 1000
- Calzetti D., Armus L., Bohlin R. C., Kinney A. L., Koornneef J., Storchi-Bergmann T., 2000, *ApJ*, 533, 682
- Chabrier G., 2003, *PASP*, 115, 763
- Croton D. J., et al., 2006, *MNRAS*, 365, 11
- Daddi E., et al., 2005, *ApJ*, 626, 680
- De Lucia G., Springel V., White S. D. M., Croton D., Kauffmann G., 2006, *MNRAS*, 366, 499
- De Lucia G., Blaizot J., 2007, *MNRAS*, 375, 2
- Dekel A., Birnboim Y., 2008, *MNRAS*, 383, 119
- Erb D. K., Steidel C. C., Shapley A. E., Pettini M., Reddy N. A., Adelberger K. L., 2006, *ApJ*, 646, 107
- Erb D. K., et al., 2014, *ApJ*, 795, 33
- Franx M., et al., 2003, *ApJ*, 587, L79
- Geach J. E., et al., 2005, *MNRAS*, 363, 1398
- Geach J. E., et al., 2014, *ApJ*, 793, 22
- Guo Q., et al., 2011, *MNRAS*, 413, 101
- Haiman Z., Rees M. J., 2001, *ApJ*, 556, 87
- Hayashino T., et al., 2004, *AJ*, 128, 2073
- Hopkins P. F., Bundy K., Murray N., Quataert E., Lauer T. R., Ma C.-P., 2009, *MNRAS*, 398, 898
- Kennicutt R. C., Jr., 1983, *ApJ*, 272, 54
- Klypin A. A., Trujillo-Gomez S., Primack J., 2011, *ApJ*, 740, 102
- Kubo M., et al., 2013, *ApJ*, 778, 170
- Kubo M., Yamada T., Ichikawa T., Kajisawa M., Matsuda Y., Tanaka I., 2015, *ApJ*, 799, 38
- Laine S., van der Marel R. P., Lauer T. R., Postman M., O'Dea C. P., Owen F. N., 2003, *AJ*, 125, 478
- Lauer T. R., 1988, *ApJ*, 325, 49
- Lehmer B. D., et al., 2009, *MNRAS*, 400, 299
- Lehmer B. D., et al., 2009, *ApJ*, 691, 687
- MacKenzie T. P., et al., 2014, *MNRAS*, 445, 201
- Matsuda Y., et al., 2004, *AJ*, 128, 569
- Matsuda Y., et al., 2005, *ApJ*, 634, L125
- Matsuda Y., Yamada T., Hayashino T., Yamauchi R., Nakamura Y., 2006, *ApJ*, 640, L123
- Matsuda Y., et al., 2009, *MNRAS*, 400, L66
- Matsuda Y., et al., 2011, *MNRAS*, 410, L13
- McLinden E. M., Malhotra S., Rhoads J. E., Hibon P., Weijmans A.-M., Tilvi V., 2013, *ApJ*, 767, 48
- Meza A., Navarro J. F., Steinmetz M., Eke V. R., 2003, *ApJ*, 590, 619
- Naab T., Khochfar S., Burkert A., 2006, *ApJ*, 636, L81
- Naab T., Johansson P. H., Ostriker J. P., Efstathiou G., 2007, *ApJ*, 658, 710
- Naab T., Johansson P. H., Ostriker J. P., 2009, *ApJ*, 699, L178
- Navarro J. F., Frenk C. S., White S. D. M., 1997, *ApJ*, 490, 493
- Oser L., Ostriker J. P., Naab T., Johansson P. H., Burkert A., 2010, *ApJ*, 725, 2312
- Osterbrock D. E., 1989, *agna.book*,
- Overzier R. A., Nesvadba N. P. H., Dijkstra M., Hatch N. A., Lehnert M. D., Villar-Martín M., Wilman R. J., Zirm A. W., 2013, *ApJ*, 771, 89
- Prescott M. K. M., et al., 2012, *ApJ*, 752, 86
- Quilis V., Trujillo I., 2012, *ApJ*, 752, L19
- Salpeter E. E., 1955, *ApJ*, 121, 161
- Seigar M. S., Lynam P. D., Chorney N. E., 2003, *MNRAS*, 344, 110
- Sloan G. C., et al., 2009, *Sci*, 323, 353
- Springel V., et al., 2005, *Natur*, 435, 629
- Steidel C. C., Adelberger K. L., Dickinson M., Giavalisco M., Pettini M., Kellogg M., 1998, *ApJ*, 492, 428
- Steidel C. C., Adelberger K. L., Shapley A. E., Pettini M., Dickinson M., Giavalisco M., 2000, *ApJ*, 532, 170
- Steidel C. C., Adelberger K. L., Shapley A. E., Pettini M., Dickinson M., Giavalisco M., 2003, *ApJ*, 592, 728
- Steidel C. C., et al., 2014, *ApJ*, 795, 165
- Stott J. P., et al., 2012, *MNRAS*, 422, 2213
- Tacconi L. J., et al., 2006, *ApJ*, 640, 228
- Tacconi L. J., et al., 2008, *ApJ*, 680, 246
- Tamura Y., et al., 2009, *Natur*, 459, 61
- Tamura Y., et al., 2013, *MNRAS*, 430, 2768
- Taniguchi Y., Shioya Y., 2000, *ApJ*, 532, L13

- Totani T., Yoshii Y., Iwamuro F., Maihara T., Motohara K., 2001, *ApJ*, 558, L87
- Trujillo I., Conselice C. J., Bundy K., Cooper M. C., Eisenhardt P., Ellis R. S., 2007, *MNRAS*, 382, 109
- Uchimoto Y. K., et al., 2008, *PASJ*, 60, 683
- Uchimoto Y. K., et al., 2012, *ApJ*, 750, 116
- Umehata H., et al., 2014, *MNRAS*, 440, 3462
- van der Wel A., et al., 2014, *ApJ*, 788, 28
- van Dokkum P. G., et al., 2008, *ApJ*, 677, L5
- Volonteri M., Haardt F., Madau P., 2003, *ApJ*, 582, 559
- Viero M. P., et al., 2012, *MNRAS*, 421, 2161
- Webb T. M. A., Yamada T., Huang J.-S., Ashby M. L. N., Matsuda Y., Egami E., Gonzalez M., Hayashino T., 2009, *ApJ*, 692, 1561
- Weijmans A.-M., Bower R. G., Geach J. E., Swinbank A. M., Wilman R. J., de Zeeuw P. T., Morris S. L., 2010, *MNRAS*, 402, 2245
- White S. D. M., Rees M. J., 1978, *MNRAS*, 183, 341
- Yamada T., Koyama Y., Nakata F., Kajisawa M., Tanaka I., Kodama T., Okamura S., De Propris R., 2002, *ApJ*, 577, L89
- Yamada T., et al., 2009, *ApJ*, 699, 1354
- Yamada T., Nakamura Y., Matsuda Y., Hayashino T., Yamauchi R., Morimoto N., Kousai K., Umemura M., 2012, *AJ*, 143, 79
- Yang Y., Zabludoff A., Tremonti C., Eisenstein D., Davé R., 2009, *ApJ*, 693, 1579
- Yang Y., et al., 2012, *ApJ*, 744, 178
- Yang Y., Zabludoff A., Jahnke K., Davé R., 2014, *ApJ*, 793, 114

**APPENDIX A: THE BEST-FIT SED MODELS
OF THE SPECTROSCOPICALLY CONFIRMED
COUNTERPARTS OF THE AZTEC14 GROUP
AND THE LABS**

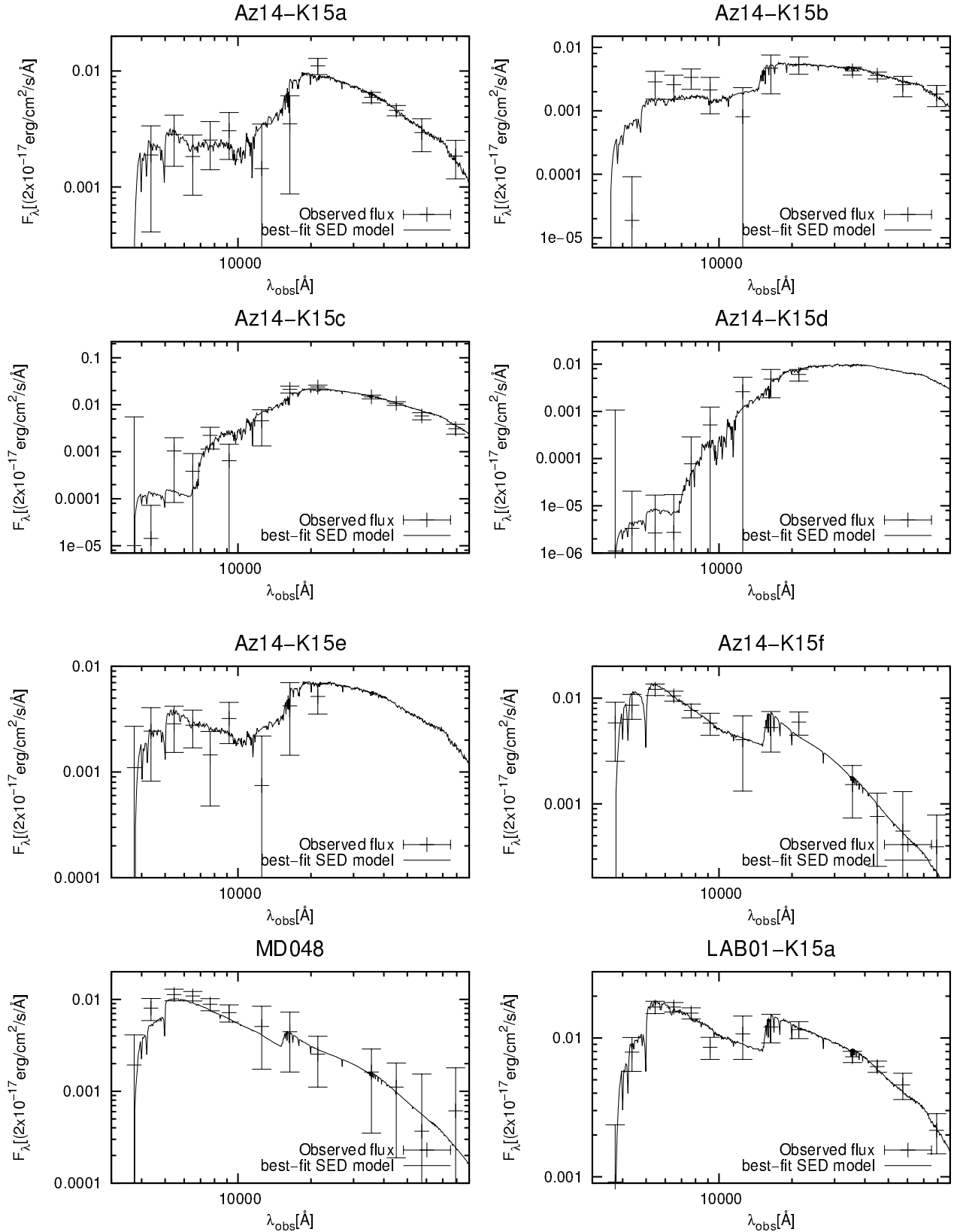


Figure A1. The observed spectra and their best-fit SEDs of the counterparts of the AzTEC14 group and the LABs. Cross points show the flux values observed in the $u^*BVRi'z'JHK$, 3.6, 4.5, 5.8 and 8.0 μm -bands. The solid lines show their best-fit SED models. At the missing data points, flux values cannot be constrained since the sources are deblended with the neighboring sources. The J -band flux values get out of the best-fit SED models largely for some objects. There is no obvious deblending but since our J -band images are very deep, it can happen that some other faint unresolved components detected in J -band only, like blue faint galaxies and $[\text{OII}] \lambda 3727$ emitters, are deblended with the central objects.

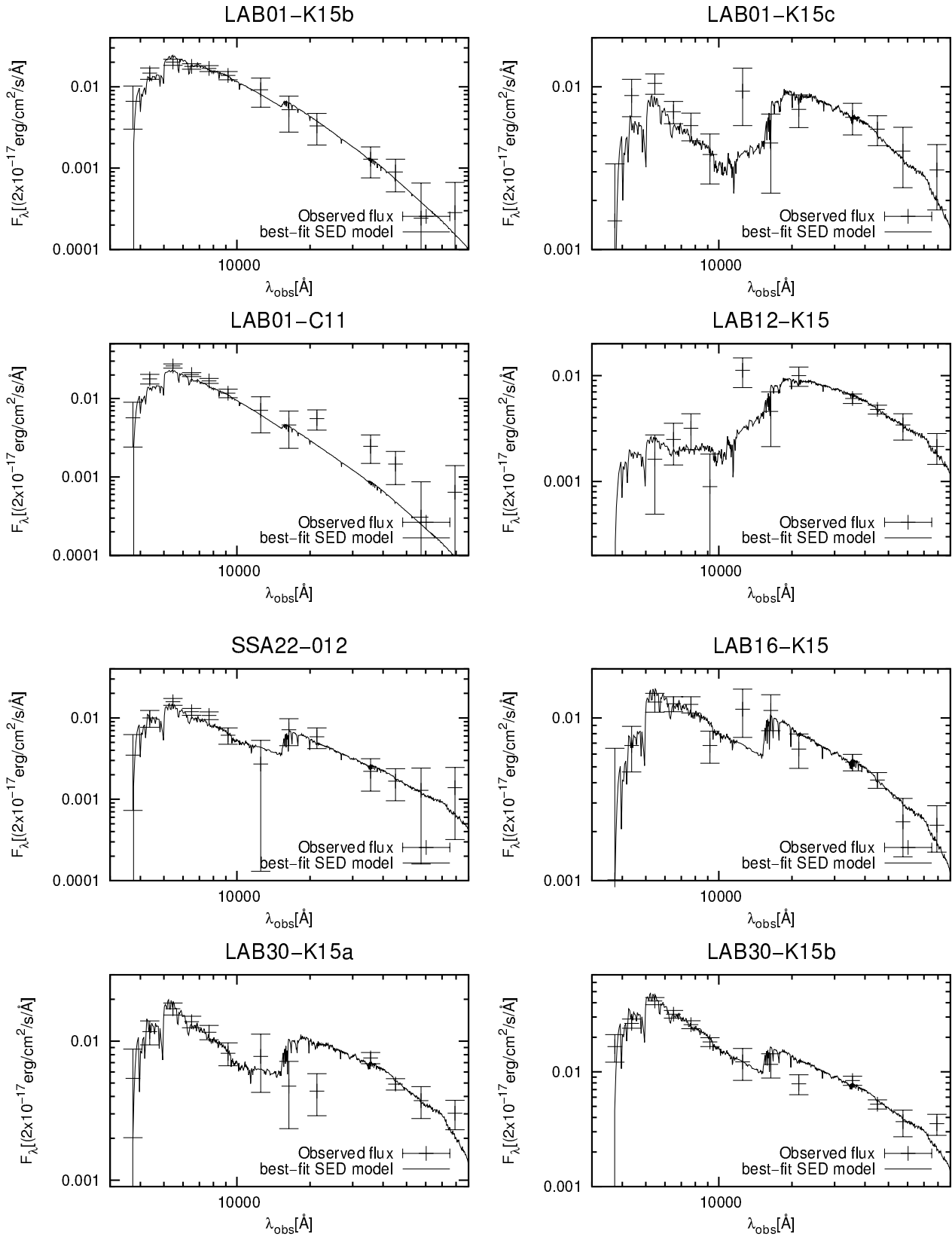


Figure A1. *Continued.*